10395
NACA TN 4061

TECH LIBRARY KAFB, NM
0067047

NATIONAL ADVISORY COMMITTEE FOR AERONAUTICS

TECHNICAL NOTE 4061

FLIGHT MEASUREMENTS OF BOUNDARY-LAYER TEMPERATURE PROFILES ON A BODY OF REVOLUTION (NACA RM-10) AT MACH NUMBERS FROM 1.2 TO 3.5

By Andrew G. Swanson, James J. Buglia, and Leo T. Chauvin

Langley Aeronautical Laboratory
Langley Field, Va.

Washington
July 1957

AFMDC
TECHNICAL LIBRARY
AFL 2811

TECH LIBRARY KAFB, NM

0067047

1H

NATIONAL ADVISORY COMMITTEE FOR AERONAUTICS

TECHNICAL NOTE 4061

FLIGHT MEASUREMENTS OF BOUNDARY-LAYER TEMPERATURE PROFILES ON A BODY OF REVOLUTION (NACA RM-10) AT MACH NUMBERS FROM 1.2 TO 3.5

By Andrew G. Swanson, James J. Buglia, and Leo T. Chauvin

SUMMARY

A fin-stabilized parabolic body of revolution, the NACA RM-10, was flight tested as a rocket-propelled model. Boundary-layer static-temperature profiles were determined from total-temperature measurements made with a series of probes mounted circumferentially around the body near the rear end and from Mach number profiles which were obtained from a total-pressure rake at the same body axial location. These static-temperature profiles showed excellent agreement with temperature profiles computed from the theory of Crocco.

Skin-friction coefficients determined from the total-pressure data by using both experimental and theoretical temperature profiles were in fair agreement with skin-friction coefficients computed from the Van Driest theory for flat plates with compressible turbulent boundary layers. Heat-transfer measurements indicated a transition from laminar to turbulent flow at a body station corresponding to a Reynolds number of about 15×10^6.

The data were obtained over a Mach number range of 1.2 to 3.5 and a Reynolds number range of 99×10^6 to 140×10^6 (based on length to the measuring station of the rake and total-temperature probes).

INTRODUCTION

The Langley Pilotless Aircraft Research Division is conducting an extensive study of skin-friction drag and aerodynamic heating at supersonic speeds by using rocket-propelled free-flight models. A systematic series of flight tests has been made with a single basic configuration, the NACA RM-10, which is a fin-stabilized parabolic body of revolution. Results of previous rocket-model tests of this configuration made by the Langley Pilotless Aircraft Research Division are reported in references 1 to 4.

As a continuation of this program, the data reported herein were obtained in order to determine the validity of the Crocco theory (ref. 5) for calculation of the temperature profile through the boundary layer; for this purpose an RM-10 rocket model was equipped with a series of total-temperature probes. The model was also equipped with a total-pressure rake for determination of average skin-friction coefficients by the momentum method. Heat-transfer data were also obtained from body skin-temperature measurements.

The data were obtained over a Mach number range of 1.2 to 3.5 and a Reynolds number range of 99×10^6 to 140×10^6 (based on length to the rake and probe station). The model was flown at the Langley Pilotless Aircraft Research Station at Wallops Island, Va.

SYMBOLS

A	parameter defined by equation (7)
b	thickness, ft
C_f	mean skin-friction coefficient
c_f	local skin-friction coefficient
c_p	specific heat at constant pressure, Btu/lb-°R
D	parameter defined by equation (13)
f	a given function
g	acceleration due to gravity, 32.2 ft/sec^2
h	local heat-transfer coefficient, $N_{St}(c_p\rho V)_l$, Btu/(sq ft)(°R)(sec)
J	mechanical equivalent of heat, 778 ft-lb/Btu
K	parameter defined by equation (9)
K_1	constant in Crocco temperature equation
K_2	constant in Crocco temperature equation
k	thermal conductivity of air, Btu-ft/(sq ft)(°R)(sec)
M	Mach number

N_{Nu}	Nusselt number, hx/k
N_{Pr}	Prandtl number, $c_p g\mu/k$
N_{St}	Stanton number, $h/c_p g\rho V$
p	pressure, lb/sq ft
$\Delta p/q$	pressure coefficient, $(p_l - p_\infty / q_\infty)$
q	dynamic pressure, lb/sq ft
R	gas constant, 53.3 ft/°R
R_l	local Reynolds number, based on distance from nose, $\frac{\rho_l V_l x}{\mu_l}$
r	distance normal to body axis, ft
r_o	body radius, ft
S	wetted area of body to measurement station, sq ft
T	temperature, °R
t	time, sec
V	velocity, ft/sec
x	axial distance along body, ft
y	distance from model wall, normal to wall, ft
γ	ratio of specific heats
δ	boundary-layer thickness, ft
δ^*	compressible flow displacement thickness, ft
μ	dynamic viscosity of air, slugs/ft-sec
ν	angle between body axis and normal to body surface
ρ	density, slugs/cu ft
θ_c	compressible flow momentum thickness, ft
τ	shearing stress, lb/sq ft

Subscripts:

av	average
aw	adiabatic wall
l	local, just outside boundary layer
s	boundary layer
t	total or stagnation
w	wall
∞	free stream

MODEL

The general configuration of the RM-10 test vehicle is shown in the sketch of figure 1 and in the photograph of figure 2. The model was basically a parabolic body of revolution having a fineness ratio of 15; however, cutting off the rear end at 81.3 percent of full length to allow for installation of a rocket motor resulted in an actual fineness ratio of 12.2. The body was stabilized by four untapered fins having an angle of sweep of 60° and an aspect ratio of 2.04. The fins had a thickness ratio of 10 percent normal to the leading edge or 5 percent in the streamwise direction.

The skin of the main body was constructed from spun magnesium-alloy sheet of 0.09-inch nominal thickness. The tail section of the body was a magnesium-alloy casting to which were welded the cast magnesium-alloy fins. The nose tip and fin leading edges were made of steel. The body was constructed with a minimum number of bulkheads and joints to keep heat-conduction losses to such items of negligible proportions. The models were polished before launching to a skin surface roughness of 50 microinches or less, as measured by a Brush profilometer. Further construction details of RM-10 rocket models are given in references 1 and 2.

INSTRUMENTATION

Boundary-layer total-temperature profiles were determined from six total-temperature probes mounted circumferentially around the body at station 125 (125 inches from nose) and extending at various heights into the boundary layer. A photograph of the installation on the model is shown in figure 3. A sketch of a typical probe is shown in figure 4.

The probe was developed by the Langley Instrument Research Division. It consisted of a chromel-alumel thermocouple junction (No. 36 gage wire) surrounded by two concentric Inconel radiation shields which were joined together at the front end by a small high-temperature silver-solder joint. A vent or "bleed" hole was located at the rear end of the external tube. The thermocouple leads were brought out through an Inconel mounting support and were insulated from the support and from one another by small ceramic disks through which the wires were led. Wind-tunnel and flight tests showed that the recovery factor of the probe was $0.997 \begin{smallmatrix}+0.003\\-0.007\end{smallmatrix}$ and that the recovery factor did not vary appreciably with Mach number (for $M_\infty > 1.0$), angle of attack (up to 30°), or ambient static pressure (1 pound per square inch absolute to 15 pounds per square inch absolute). The bleed area of the probe was 27 percent of the entrance area. The time constant was about 0.11 second and did not vary over the Reynolds number range of the present test. Only the innermost probe measured total temperature directly. The other probes measured differential temperatures from one probe to the next. The accuracy of the direct-measurement probe was about ±22° R (based on ±2 percent of full-scale range). The other probes were each subject to an additional error of about ±5° R (±2 percent of full-scale differential range); however, these errors would not be expected to be cumulative but should total approximately zero for the summed readings since these additional errors should be randomly distributed from probe to probe.

The model had a six-tube total-pressure rake, sketched in figure 5, mounted at the same body station (station 125) as the total-temperature probes. The tubes were constructed of stainless steel and are further described in reference 1. Again, only the innermost tube measured total quantity, and the outer tubes measured differential total pressures from tube to tube. The pressure data should be accurate to within ±0.6 pound per square inch gage and ±0.4 pound per square inch gage for the absolute and differential pressures, respectively.

Skin temperatures were measured at body stations 18, 45, 72, 100, and 125 by means of chromel-alumel thermocouples (No. 30 gage wire) welded in the skin. These temperature data should be accurate to within about ±10° R (approximately 2 percent of the full-scale thermocouple range).

Measurements of temperatures, pressures, and longitudinal accelerations of the test vehicle were transmitted to the ground from a standard NACA telemeter located in the nose of the model. Atmospheric data, including wind velocity, were obtained from a Rawin set AN/GMD-1A (a radar-tracked sounding balloon). Model space position was obtained by an NACA modified SCR-584 tracking radar. Model velocity over a part of the flight test was measured by a CW Doppler radar set.

TEST AND ANALYSIS

Flight

The model was ground launched at an angle of 75°. A photograph of the model on the launcher is shown in figure 6. A booster consisting of two ABL Deacon rocket motors firing simultaneously accelerated the test vehicle to a Mach number of approximately 1.6. The booster then drag-separated from the model, and, after a period of coasting flight lasting approximately 10 seconds, a third Deacon rocket motor mounted within the test vehicle was fired and the vehicle was accelerated from a Mach number of about 0.95 to a peak Mach number of about 3.5. The vehicle then decelerated in coasting flight. Data were recorded during both the powered and the coasting portions of the flight. Throughout the entire flight the model followed essentially a zero-lift trajectory, as is evidenced by comparison of the actual trajectory with a calculated zero-lift trajectory.

Free-Stream Conditions

Ambient conditions measured by the radiosonde balloon as functions of altitude were converted to time histories of free-stream conditions along the flight path by combining the radiosonde data with the model trajectory determined by the SCR-584 space radar set. Model velocity was determined from Doppler radar data until about 4 seconds after peak speed was reached (or until the model had decelerated to a Mach number of about 3.0). After this time, velocity was determined from integration of the telemetered longitudinal accelerations. Free-stream atmospheric data were combined with the velocity data to give the time histories of free-stream Mach number and Reynolds number.

Local Flow Conditions

Local flow conditions over the body, expressed as functions of the free-stream Mach number and ratios of free-stream to local conditions, were determined from composite plots of data from previous flight and wind-tunnel tests of the RM-10 which agree with computations by the method of characteristics used for intermediate Mach numbers.

Rake Pressure Measurements

With the usual assumption of constant static pressure throughout the boundary layer, the Mach number profile throughout the boundary layer was computed from the rake total-pressure data, static pressure determined from the local flow conditions, and normal-shock tables. Some of the Mach numbers computed for the outermost rake positions did not agree with the local Mach numbers computed from the free-stream Mach numbers and local flow conditions. In all cases of disagreement, the rake data gave local Mach numbers higher than did the local flow computations. The magnitude of the differences ($\Delta M \leq 0.05$) was generally within the determined accuracy of the data. The pressure lag was checked and was found to be negligible for the given rates of change of pressure.

This difference, however, could not be caused by errors of reasonable size in the determination of free-stream velocity, ambient conditions, or local flow conditions (including local static pressure). Therefore, the rake data were assumed to be the chief sources of disagreement. Since a source of error in any one rake-tube measurement could not be located, the arbitrary assumption was made that only the outermost tube or, in some cases, the two outermost tubes were in error, and the Mach number profiles were adjusted to make the Mach numbers from the outermost tubes and local flow conditions agree (since free-stream Mach number and local flow conditions were believed to be reasonably accurate).

Rake Temperature Measurements

A line was faired through the measured total-temperature data to determine the total-temperature profiles throughout the boundary layer. This faired curve was combined with the faired Mach number profiles to determine velocity and static-temperature profiles from the usual isentropic flow relations. The temperature data from the outermost probes generally showed excellent agreement with free-stream stagnation temperature; the differences between the two sets of data were essentially zero for about one-half the points computed and within the accuracy of the experimental data ($\pm 22^{\circ}$ R) for the remaining points except at 16.45 and 28.00 seconds, for which the differences were 26° and -23° R, respectively.

Theoretical temperature profiles were obtained by use of the Crocco theory (ref. 5) which was solved as shown in the appendix for

$$\frac{T}{T_l} = f\left(T_w, T_l, T_t, M, M_l\right)$$

These temperature profiles were combined with the experimental Mach number profiles to give a velocity distribution through the boundary layer.

Boundary-layer thickness was determined from logarithmic plots of nondimensional velocity V/V_l against y/δ.

Skin-Friction Coefficients

Skin-friction coefficients were obtained by using both theoretical and experimental temperature profiles from the momentum equations as shown in the appendix. Values of skin-friction coefficient were also obtained from the theory of Van Driest (refs. 6 to 8) at all times for which rake data were reduced. Local values of skin-friction coefficient were computed from theory at each of the body stations where wall temperature was measured by using local flow conditions. These coefficients were integrated over the area of the RM-10 body ahead of station 125 (the location of temperature and pressure probes) to obtain an average skin-friction coefficient up to station 125. The use of the flat-plate theory was considered admissible for the RM-10 body of revolution since its diameter is large in comparison with the boundary-layer thickness, the apex angle is small, and the surface in the vicinity of station 125 is practically cylindrical.

Stanton Number

Skin-temperature data were reduced to heat-transfer coefficients by use of a conventional heat-balance relation:

$$h = N_{St}\left(c_p\rho V\right)_l = \frac{\left(c_p\rho b\right)_w}{T_{aw} - T_w}\frac{dT_w}{dt}$$

The effects of radiation and conduction along the body have been neglected since calculations showed them to be negligible. The adiabatic-wall temperature was computed from the usual relation for a turbulent boundary layer:

$$T_{aw} = T_l + N_{Pr}^{1/3}\left(T_t - T_l\right)$$

in which N_{Pr} was based on wall temperature. The specific heat of magnesium as a function of temperature was obtained from reference 9.

RESULTS AND DISCUSSION

Shown in figure 7 are the ambient atmospheric conditions encountered by the model during the time for which data are presented. Figure 8 shows time histories of free-stream Mach number and Reynolds number. Also indicated in figure 8 are the times for which temperature profiles and skin-friction coefficients were computed. Temperatures of the body skin are shown as time histories in figure 9.

Boundary-Layer Profiles

The experimentally determined Mach number and total-temperature data are presented in figure 10 as nondimensional plots of $\frac{M}{M_l}$ and $\frac{T_t}{T_{t,l}}$ through the boundary layer y. The experimental points determined directly from the rake data are shown together with the curves faired through these points; the faired curves were used in further reduction of the data. The data are presented for the various times during the flight for which data were reduced. Shown in the figure are the values, at each value of time, of local Mach number (just outside the boundary layer), wall heating condition (expressed by the ratio T_w/T_{aw}), free-stream total temperature, and the local boundary-layer thickness for the rake measuring station (body station 125).

The physical size of the rake and probes prevented measurements closer to the skin than 0.06 inch in the case of the total-pressure rake and 0.13 inch in the case of the total-temperature probe. Inasmuch as the fairing of the profiles between the wall and the innermost data point would be fairly arbitrary, no curve was faired through this region. The extension of the outer probes beyond the nominal boundary-layer thickness is readily apparent as are the generally smaller differences between the local Mach numbers and total temperature determined from the rake and probe data and those determined from local flow conditions. As noted in the section entitled "Instrumentation," the probes measured the actual total temperature at the innermost position only, and the remainder of the profile was measured by differential readings from probe to probe. Therefore, the apparent displacement of the experimental data from the faired curve throughout the entire curve (fig. 10(n), for example) is probably due to an error in the innermost or absolute probe. The discrepancy in the temperature data at 28 seconds only slightly exceeds the anticipated accuracy of the data and at lower values of time (for example, 5.59 or 8.46 seconds (figs. 10(c) and 10(d), respectively)) the disagreement is well within the probable limits of accuracy.

Except at 28.00 and 34.17 seconds, the skin is always cooler than the adiabatic-wall temperature; however, as would be expected, the amount of heating potential, expressed by the ratio T_w/T_{aw}, affects the shape of the temperature curves. Note that this wall-temperature condition applies only to the measuring station (station 125).

Indicated by arrows in figure 10 are the values of M/M_l corresponding to a Mach number of 1 within the boundary layer. The boundary layer can be seen to be largely supersonic; in fact, for values of local Mach number greater than about 2.0, the boundary layer is essentially all supersonic, the subsonic layer being less than about 3 percent of the total boundary-layer thickness.

The nondimensional velocity and static-temperature profiles determined from the data of figure 10 are shown in figure 11 together with profiles predicted from the Crocco theory (ref. 5). The experimental values shown in this figure were not determined directly from the rake data but were determined from the curves faired through the experimental Mach number distribution of figure 10.

The agreement between theory and experiment is excellent; most of the experimental points are in exact agreement with the theoretical curves and most of the small differences exhibited by the remaining points are within the accuracy of the experimental data. Therefore, within the range of flight conditions of this and other RM-10 research missiles previously investigated (refs. 1 and 3), the Crocco theory adequately predicts the actual static-temperature distribution throughout the turbulent boundary layer.

Inasmuch as the Mach number could not be measured close to the wall, velocity and temperature profiles were not calculated for values of y/δ of less than about 0.04. Since, during the times when the skin is being heated, the static temperature adjacent to the skin is greater than T_w, the static-temperature profile would then have a positive slope in this region; the value of the slope would vary inversely with the amount of heating.

Because the same experimentally determined Mach number profiles were used to obtain both the experimental and the theoretical temperature and velocity profiles, any errors in the Mach number data would affect both theoretical and experimental results in a similar fashion; therefore, the fairing of the total-pressure-rake data (see section entitled "Test and Analysis") would not affect the comparison between the Crocco theory and the experimental results.

Also shown in figure 11 are the velocity profiles computed from $\frac{V}{V_l} = \left(\frac{y}{\delta}\right)^{1/7}$ ("1/7-power" law). This relation gives good results for some of the data although it does not give the true velocity distribution for every compressible turbulent boundary layer.

Skin-Friction Coefficients

The rake data were reduced to skin-friction coefficients as shown in the appendix, and the results are presented in figure 12. The experimental results are compared with skin-friction coefficients predicted from the theory of Van Driest (ref. 6 modified as suggested in ref. 7) for flat plates with compressible turbulent heat transfer. Since the temperature data indicated transitional flow over the nose of the model, theoretical values of C_f were also computed by using the theory of reference 8 with the assumption of laminar flow extending to the transition station (station 18). There was essentially no difference in the integrated average skin friction computed by the two methods (without laminar flow and with laminar flow), mainly because of the small percentage of the body area between station 18 and the nose.

As shown in figure 12, the general level of the experimental data is in fair agreement with the Van Driest theory (ref. 6). These results are compatible with the data of reference 10, which also indicated fair agreement with the Van Driest theory for skin friction on the RM-10 body. The experimental point at $M = 3.2$ which seems out of line is at the time (15.99 seconds) when the experimental temperature profile shows some difference from the theoretical profile for some distance through the boundary layer. At $M = 2.28$ and 2.05, the experimental data are approaching maximum unreliability since they were obtained late in the flight (28.00 and 34.17 seconds, respectively). Another source of the discrepancy, however, possibly lies in the fact that at these times the boundary layer was thinnest; therefore, the temperature and velocity profiles could not be computed at so low values of y/δ as was possible at the earlier times. The experimental skin-friction coefficients C_f showing closest agreement with the Van Driest data were generally obtained at those times when the boundary-layer thickness was greatest. Also shown as circled points in figure 12 are the values of C_f computed with the Crocco temperature and velocity profiles (based on experimental Mach number profiles); the general trend of these points from the Crocco theory is in agreement with skin-friction-coefficient data from the Van Driest theory. The Crocco datum points show somewhat closer agreement with those of the Van Driest theory than do the experimental temperature-profile datum points.

Heat-Transfer Coefficients

The body skin temperatures shown in figure 9 were reduced to heat-transfer coefficients. These heat-transfer data are shown in figure 13 as a correlation plot which gives $\frac{N_{Nu}}{N_{Pr}^{1/3}}$ as a function of local Reynolds number. Also shown in this figure is a curve computed from the heat-transfer theory of Van Driest (ref. 6 modified in accordance with ref. 7) for turbulent boundary layers. Laminar heat-transfer theory, also from Van Driest (ref. 8) is given by the lower curve. The value of N_{St} was considered to be $0.6c_f$, as indicated in reference 11. Transitional flow existing to at least station 18 is indicated. The scatter of the data is of the order of 30 percent but the general level of the data is in agreement with the Van Driest turbulent theory (except at the transitional-flow points). The experimental heat-transfer data are in fair agreement with the curve from reference 4. The present test data show better agreement with the data from reference 4 if the mass of points from that reference is considered. The present test has more data at Reynolds numbers of approximately 2.5×10^6 which, when considered with the reference data, would alter the faired curve of reference 4 at the lower Reynolds numbers and would make the experimental data of the present and the reference investigations agree fairly well for all Reynolds numbers presented. The transition Reynolds number indicated by the data of figure 13 is about 15×10^6.

The skin-temperature instrumentation was installed primarily for the purpose of preliminary determination of the validity of Reynolds analogy as applied to nonisothermal surfaces (as was also done in ref. 3). Reference 12 states that, theoretically, Reynolds analogy does not apply to surfaces having a variable (with surface distance) temperature distribution.

The scatter in the data evident in figure 13 precluded the attempt to determine the validity of Reynolds analogy for the surface-temperature distributions encountered in this investigation; no conclusion could be drawn from the comparison of heat-transfer coefficients integrated over the RM-10 surface with the skin-friction data from the rake measurements. However, since the theoretical Van Driest heat-transfer data make use of the Reynolds analogy to reduce C_f to N_{St}, and since the experimental data scatter about the level of the Van Driest curve, the Reynolds analogy still seems to be valid for skin-temperature distributions encountered in this test. Reference 3 also indicates that Reynolds analogy applies for such conditions.

CONCLUDING REMARKS

A parabolic body of revolution, the NACA RM-10, was flight tested as a rocket-propelled vehicle. Boundary-layer-temperature profiles determined from total-temperature probes showed excellent agreement with profiles predicted from the theory of Crocco. Skin-friction coefficients determined by the momentum method from total-pressure-rake data were in fair agreement with the Van Driest theory for flat plates with compressible turbulent boundary layers. Heat-transfer measurements indicated a transition Reynolds number (laminar to turbulent flow) of about 15×10^6. The data were obtained over a Mach number range of 1.2 to 3.5 and a Reynolds number range of 99×10^6 to 140×10^6 (based on length to the rake and probe measuring station).

Langley Aeronautical Laboratory,
National Advisory Committee for Aeronautics,
Langley Field, Va., April 29, 1957.

APPENDIX

DERIVATION OF EQUATIONS USED IN DATA REDUCTION

Temperature Equation

The theoretical static-temperature distribution through the boundary layer was evaluated by using the relation given by Crocco in reference 5, which gives the temperature as a function of velocity. The relation used was

$$T = K_1 + K_2 V - \frac{V^2}{2Jgc_p} \tag{1}$$

with the boundary conditions

$$\left.\begin{aligned} T &= T_l \qquad (V = V_l) \\ T &= T_w \qquad (V = 0) \end{aligned}\right\} \tag{2}$$

Substitution of the boundary conditions gives

$$T = T_w + \frac{V}{V_l}\left(T_l - T_w\right) + \frac{V}{V_l}\frac{{V_l}^2}{2Jgc_p} - \frac{V^2}{2Jgc_p} \tag{3}$$

Using the definition of total temperature

$$T_{t,\infty} = T_{t,l} = T_l + \frac{{V_l}^2}{2Jgc_p} \tag{4}$$

gives equation (3) the form

$$T = T_w + \frac{V}{V_l}\left(T_t - T_w\right) - \frac{V^2}{2Jgc_p} \tag{5}$$

Adding $T_l + \frac{V_l^2}{2Jgc_p}$, subtracting T_t, and collecting terms give the equation in final form as

$$T = T_l + \left(T_w - T_t\right)\left(1 - \frac{V}{V_l}\right) + \frac{\left(V_l^2 - V^2\right)}{2Jgc_p} \tag{6}$$

Equation (6) is similar to the expression used in reference 1 except that the recovery factor has been taken to be 1.0. Calculations show that the use of a recovery factor of 1.0 gives better agreement with the actual energy variation through the boundary layer than does a recovery factor of approximately $N_{Pr}^{1/3}$, even though the latter better satisfies the boundary conditions at the wall under thermal equilibrium conditions.

Since, on most RM-10 models, the Mach number profile through the boundary layer was measured by total-pressure rakes, the static-temperature variation through the boundary layer may be expressed conveniently in terms of Mach number. Therefore, let

$$A \equiv \frac{1}{2Jgc_p} \tag{7}$$

and

$$T = \frac{V^2}{\gamma gRM^2} = \frac{V^2}{KM^2} \tag{8}$$

where

$$K \equiv \gamma gR \tag{9}$$

With the substitution of equations (7) and (8) into equation (6) and the notation that

$$AV_l^2 = T_t - T_l \tag{10}$$

equation (6) becomes

$$\left(\frac{1}{KM^2} + A\right) V_l^2 \frac{V^2}{V_l^2} + \left(T_w - T_t\right)\frac{V}{V_l} - T_w = 0 \tag{11}$$

which is quadratic in V/V_l.

Equation (11) may be solved by the quadratic formula

$$\frac{V}{V_l} = \frac{-D \pm \sqrt{D^2 + \frac{T_w}{T_t - T_l}\left(\frac{1}{AKM^2} + 1\right)}}{\left(\frac{1}{AKM^2} + 1\right)} \tag{12}$$

in which

$$D \equiv -\frac{1}{2}\left(\frac{T_w - T_t}{T_t - T_l}\right) \tag{13}$$

For the conditions

$$\gamma = 1.4 \qquad J = 778\ \frac{\text{ft-lb}}{\text{Btu}}$$

$$R = 53.3\ \text{ft/}^{\circ}\text{R} \qquad c_p = 0.24\ \frac{\text{Btu}}{\text{lb-}^{\circ}\text{R}}$$

$$g = 32.2\ \text{ft/sec}^2 \qquad AK = \frac{\gamma g R}{2Jgc_p} = 0.20$$

equation (12) becomes

$$\frac{V}{V_l} = \frac{-D \pm \sqrt{D^2 + \frac{T_w}{T_t - T_l}\left(\frac{1}{0.2M^2} + 1\right)}}{\left(\frac{1}{0.2M^2} + 1\right)} \tag{14}$$

Then, the temperature distribution is found as

$$\frac{T}{T_l} = \left(\frac{V}{V_l}\frac{M_l}{M}\right)^2 \tag{15}$$

Momentum Equation

The boundary-layer momentum equation for a body of revolution is given in reference 13 as

$$\frac{\partial}{\partial x}\int_0^\delta \rho V^2 r\ dy - V_l \frac{\partial}{\partial x}\int_0^\delta \rho V r\ dy = -\tau_w r_o - \frac{\partial p}{\partial x}\int_0^\delta r\ dy \tag{16}$$

where the expression in reference 13 is modified by setting $\cos \nu = 1$ and $r = r_o + y$; ν is the angle between the normal to the body surface and the normal to the axis of revolution. In addition, x is measured along the body axis rather than along the surface. These simplifying assumptions are valid since the radius of curvature of the RM-10 body is fairly large.

As noted in reference 13,

$$-\frac{\partial p}{\partial x} = \rho_l V_l \frac{\partial V_l}{\partial x} \tag{17}$$

therefore,

$$\tau_w r_o = V_l \frac{\partial}{\partial x}\int_0^\delta \rho V r\ dy - \frac{\partial}{\partial x}\int_0^\delta \rho V^2 r\ dy + \rho_l V_l \frac{\partial V_l}{\partial x}\int_0^\delta r\ dy \tag{18}$$

From the relation

$$V_l \frac{\partial}{\partial x}\int_0^\delta \rho V r\ dy = \frac{\partial}{\partial x}\int_0^\delta \rho V V_l r\ dy - \frac{\partial V_l}{\partial x}\int_0^\delta \rho V r\ dy \tag{19}$$

and the definitions of boundary-layer displacement and momentum thickness for a body of revolution (ref. 13)

$$\delta^* = \int_0^\delta \frac{r}{r_o}\left(1 - \frac{\rho V}{\rho_l V_l}\right) dy \tag{20}$$

$$\theta_c = \int_0^\delta \frac{r}{r_o}\left(1 - \frac{V}{V_l}\right)\left(\frac{\rho V}{\rho_l V_l}\right)dy \tag{21}$$

the conventional notation is obtained for the momentum equation of a body of revolution with a pressure gradient:

$$\tau_w r_o = \frac{\partial}{\partial x}\left(r_o \rho_l V_l^2 \theta_c\right) + \frac{\partial V_l}{\partial x}\left(r_o \rho_l V_l \delta^*\right) \tag{22}$$

The mean skin-friction coefficient is

$$C_f = \frac{\tau_{w,av}}{\frac{1}{2}\rho_\infty V_\infty^2} = \frac{2\pi}{\frac{1}{2}\rho_\infty V_\infty S}\int_0^x \tau_w r_w \, dy \tag{23}$$

For convenience in computation, equation (23) is rewritten as

$$C_f = \frac{4\pi}{S\rho_\infty V_\infty^2}\left[\rho_l V_l^2 \int_0^\delta \frac{\rho V}{\rho_l V_l}\left(1 - \frac{V}{V_l}\right) r \, dy + \int_0^x \rho_l V_l r_o \delta^* \frac{\partial V_l}{\partial x} \, dx\right] \tag{24}$$

where use is made of equations (21) and (22).

Since the static pressure is constant throughout the boundary layer,

$$\frac{\rho V}{\rho_l V_l} = \frac{V_l}{V}\left(\frac{M}{M_l}\right)^2$$

and equation (24) can be written in final form as

$$C_f = \frac{4\pi}{S}\frac{\rho_l V_l^2}{\rho_\infty V_\infty^2}\int_0^\delta \left(\frac{M}{M_l}\right)^2\left(\frac{V_l}{V} - 1\right) r \, dy + \frac{4\pi}{S}\frac{1}{\rho_\infty V_\infty^2}\int_0^x \rho_l V_l r_o \delta^* \frac{\partial V_l}{\partial x} \, dx \tag{25}$$

By assuming a linear variation of δ^* with x from a value of zero at the nose to the value at the measuring station, the terms of equation (25) can readily be evaluated from the rake data and experimental or Crocco theory static-temperature profiles. In order to simplify computations further, the second integral was evaluated as a percentage of the first integral (as a function of M_∞) for several previous RM-10 models. The second integral varies from 4 to 9 percent of the first over the Mach number range from 1.0 to 3.5 and can be determined to within $1\frac{1}{2}$ percent of the first integral by use of data plotted from the previous RM-10 models.

REFERENCES

1. Rumsey, Charles B., and Loposer, J. Dan: Average Skin-Friction Coefficients From Boundary-Layer Measurements in Flight on a Parabolic Body of Revolution (NACA RM-10) at Supersonic Speeds and at Large Reynolds Numbers. NACA RM L51B12, 1951.

2. Chauvin, Leo T., and deMoraes, Carlos A.: Correlation of Supersonic Convective Heat-Transfer Coefficients From Measurements of the Skin Temperature of a Parabolic Body of Revolution (NACA RM-10). NACA TN 3623, 1956. (Supersedes NACA RM L51A18.)

3. Maloney, Joseph P.: Drag and Heat Transfer on a Parabolic Body of Revolution (NACA RM-10) in Free Flight to Mach Number 2 With Both Constant and Varying Reynolds Number and Heating Effects on Turbulent Skin Friction. NACA RM L54D06, 1954.

4. Chauvin, Leo T., and Maloney, Joseph P.: Turbulent Convective Heat-Transfer Coefficients Measured From Flight Tests of Four Research Models (NACA RM-10) at Mach Numbers From 1.0 to 3.6. NACA RM L54L15, 1955.

5. Crocco, Luigi: Transmission of Heat From a Flat Plate to a Fluid Flowing at a High Velocity. NACA TM 690, 1932.

6. Van Driest, E. R.: The Turbulent Boundary Layer for Compressible Fluids on a Flat Plate With Heat Transfer. Rep. No. AL-997, North American Aviation, Inc., Jan. 27, 1950.

7. Van Driest, E. R.: The Turbulent Boundary Layer With Variable Prandtl Number. Rep. No. AL-1914, North American Aviation, Inc., Apr. 2, 1954.

8. Van Driest, E. R.: Investigation of Laminar Boundary Layer in Compressible Fluids Using the Crocco Method. NACA TN 2597, 1952.

9. Kelley, K. K.: Contributions to the Data on Theoretical Metallurgy. II. High-Temperature Specific-Heat Equations for Inorganic Substances. Bulletin 371, Bur. Mines, 1934, p. 32.

10. Rubesin, Morris W., Rumsey, Charles B., and Varga, Steven A.: A Summary of Available Knowledge Concerning Skin Friction and Heat Transfer and Its Application to the Design of High-Speed Missiles. NACA RM A51J25a, 1951.

11. Rubesin, Morris W.: A Modified Reynolds Analogy for the Compressible Turbulent Boundary Layer on a Flat Plate. NACA TN 2917, 1953.

12. Ferrari, Carlo: Determination of the Heat Transfer Properties of a Turbulent Boundary Layer in the Case of Supersonic Flow When the Temperature Distribution Along the Constraining Wall is Arbitrarily Assigned. Rep. No. CAL/CM-807 (Contract NOrd-14523), Cornell Aero. Lab., Inc., Mar. 1954.

13. Young, A. D.: Boundary Layers. Vol. I of Modern Developments in Fluid Dynamics - High Speed Flow, L. Howarth, ed., The Clarendon Press (Oxford), 1953, pp. 375-475.

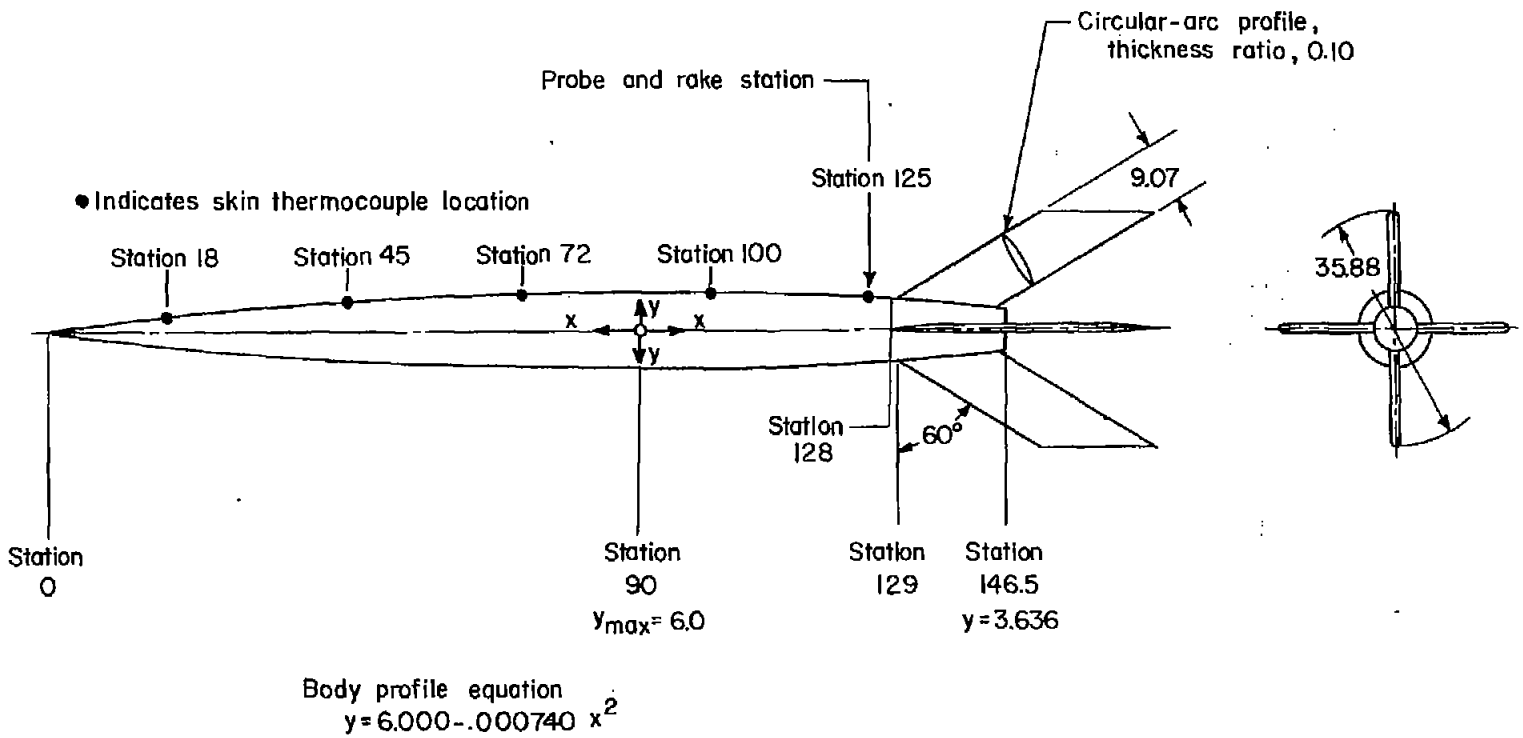

Figure 1.- General configuration and body equation of NACA RM-10. All dimensions are in inches.

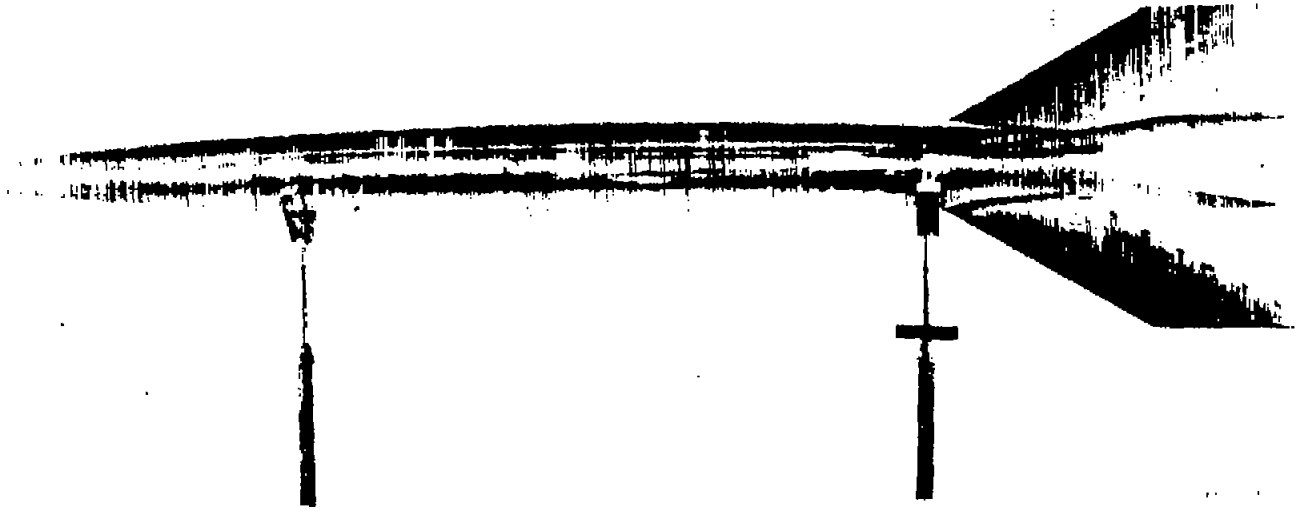

L-84099

Figure 2.- Photograph of test vehicle.

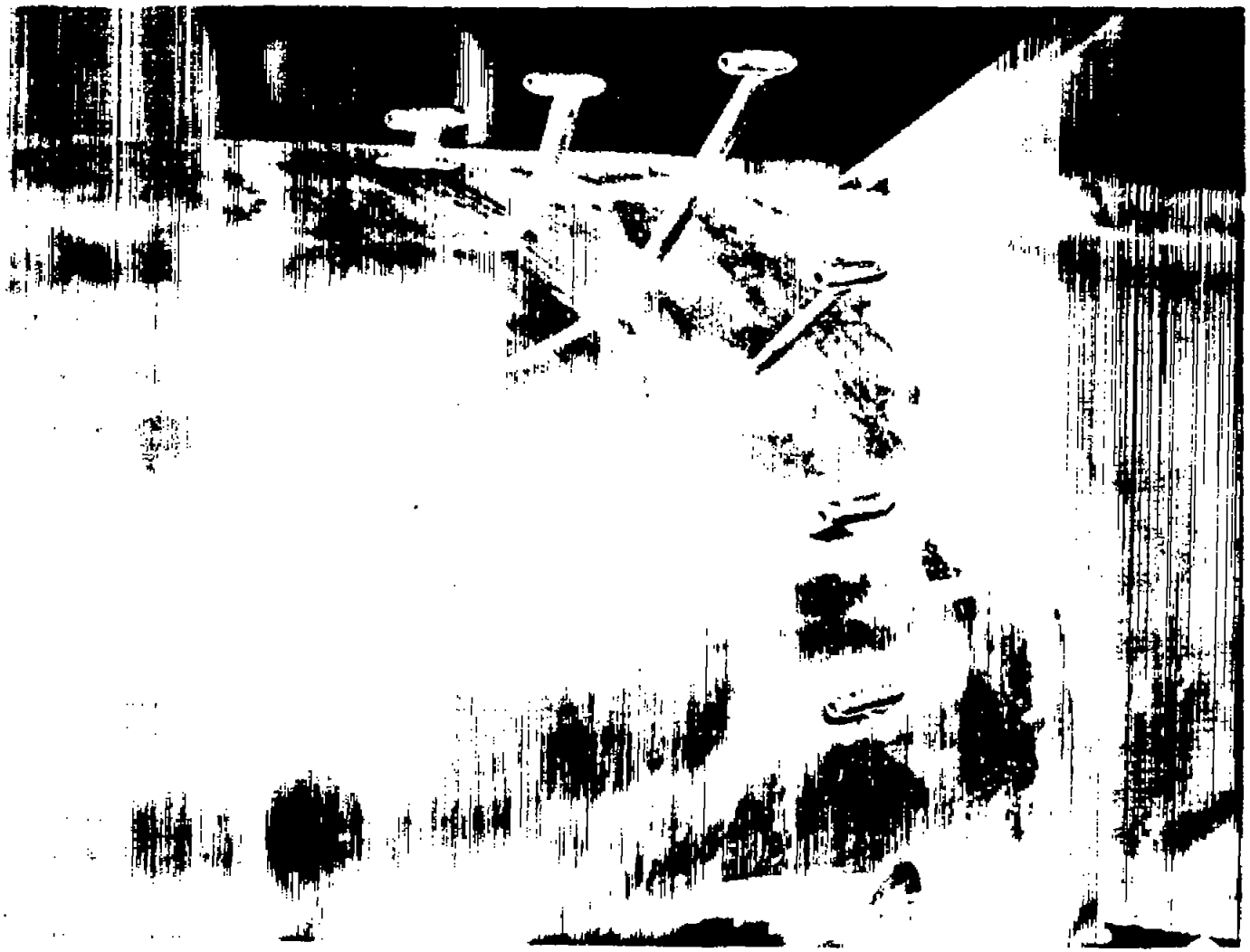

L-84098

Figure 3.- Photograph of total-temperature-probe installation.

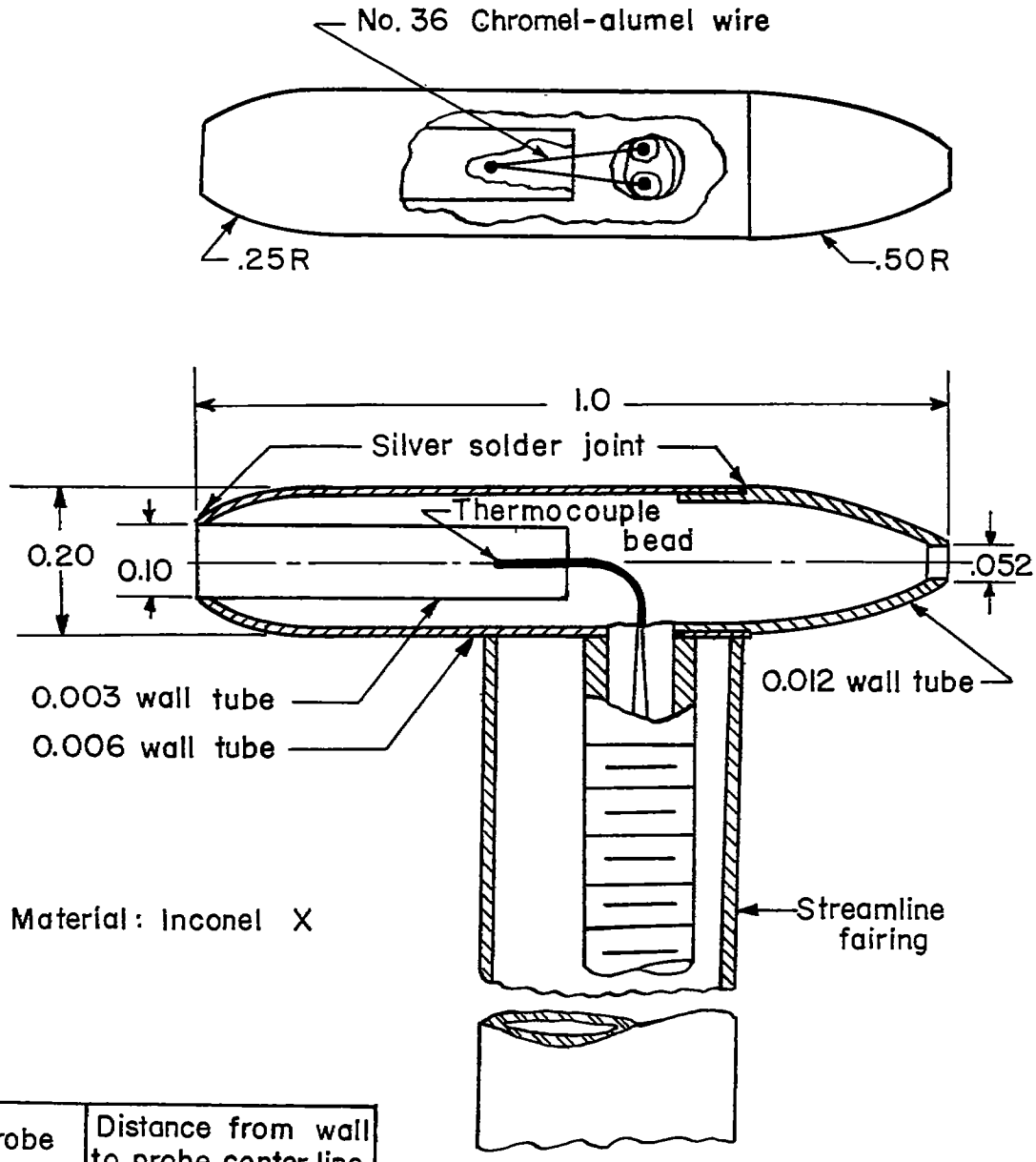

Probe	Distance from wall to probe center line
1	0.130
2	.235
3	.483
4	.900
5	1.403
6	1.990

Figure 4.- Stagnation-temperature probe. All dimensions are in inches.

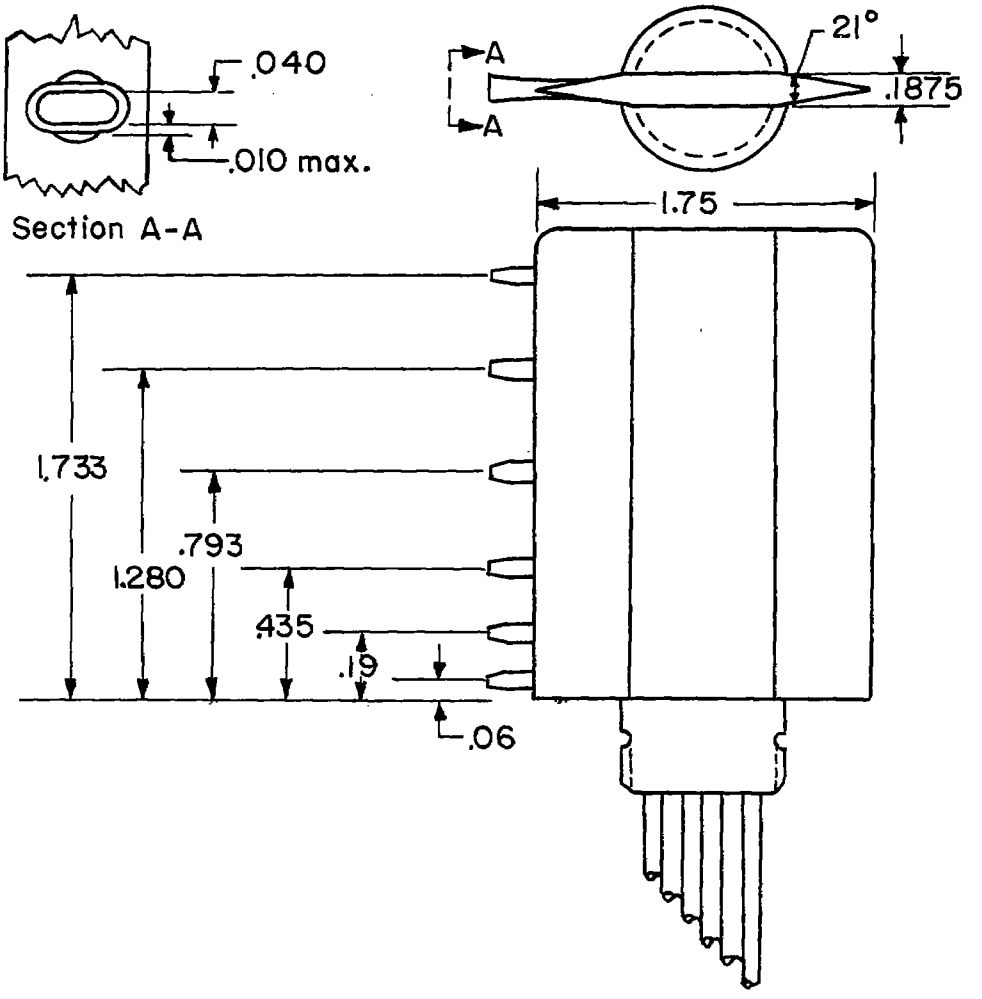

Figure 5.- General configuration of total-pressure rakes and spacing of tubes. All dimensions are in inches.

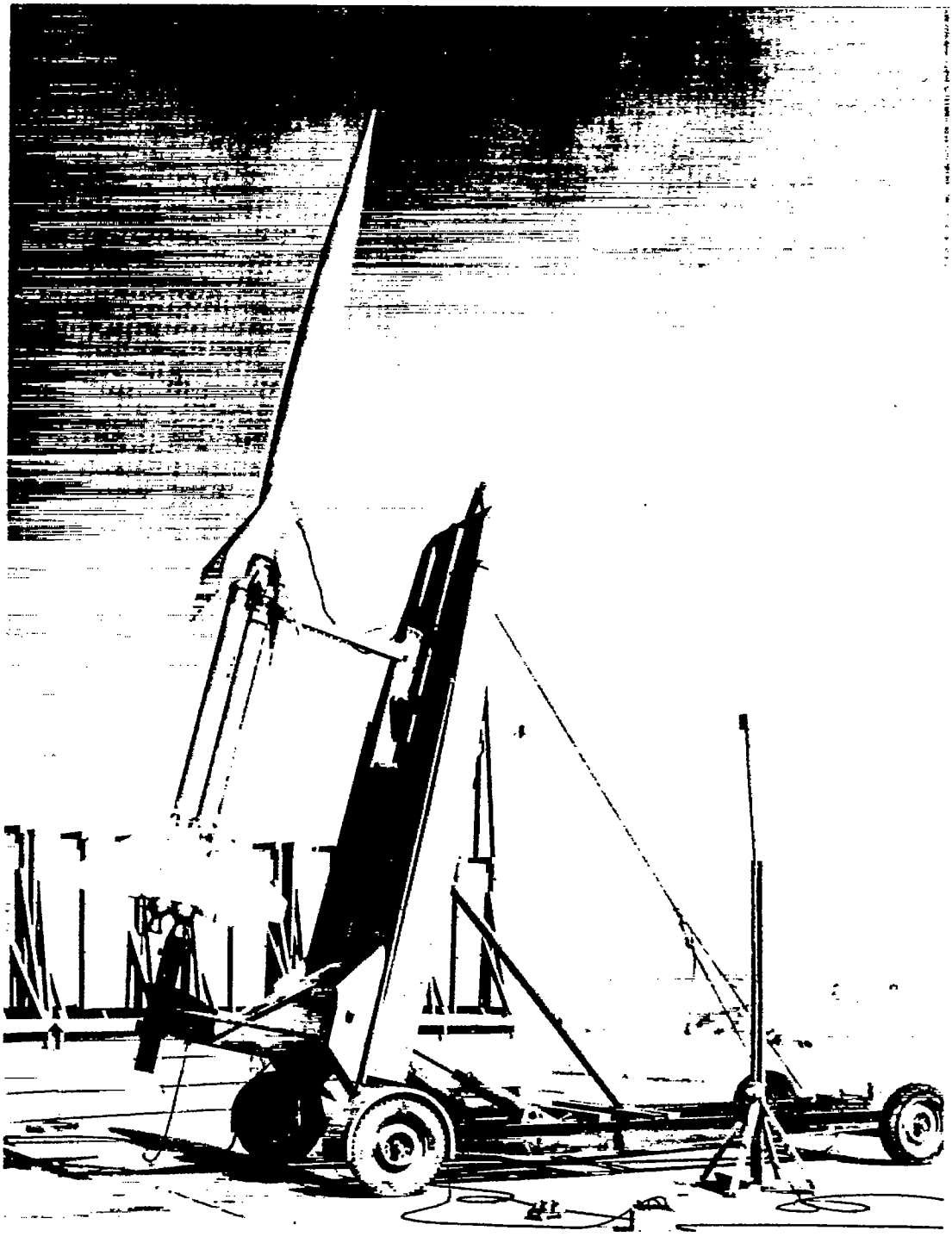

L-84534.1

Figure 6.- Photograph of model and booster on launcher.

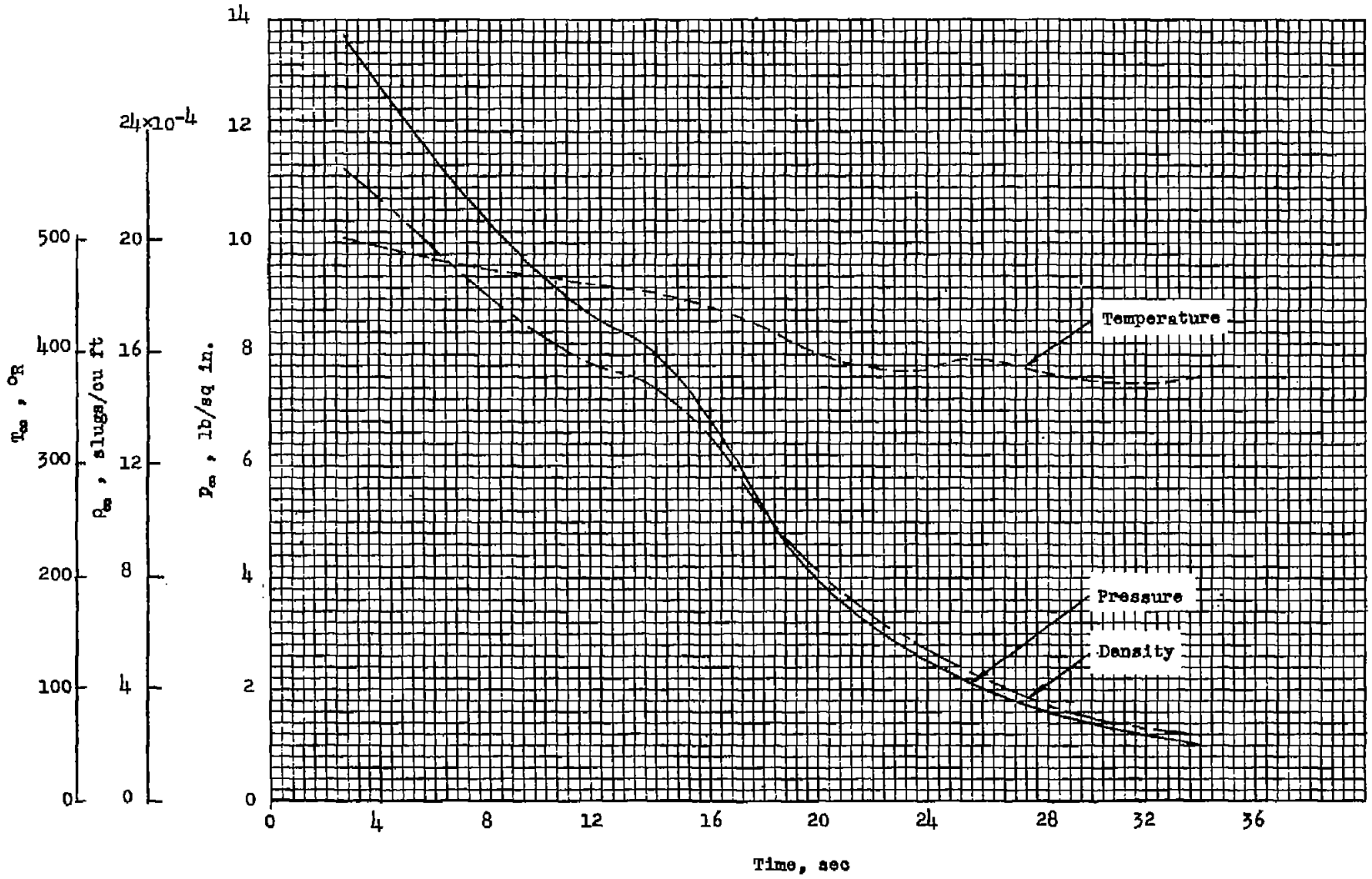

Figure 7.- Time histories of ambient atmospheric conditions.

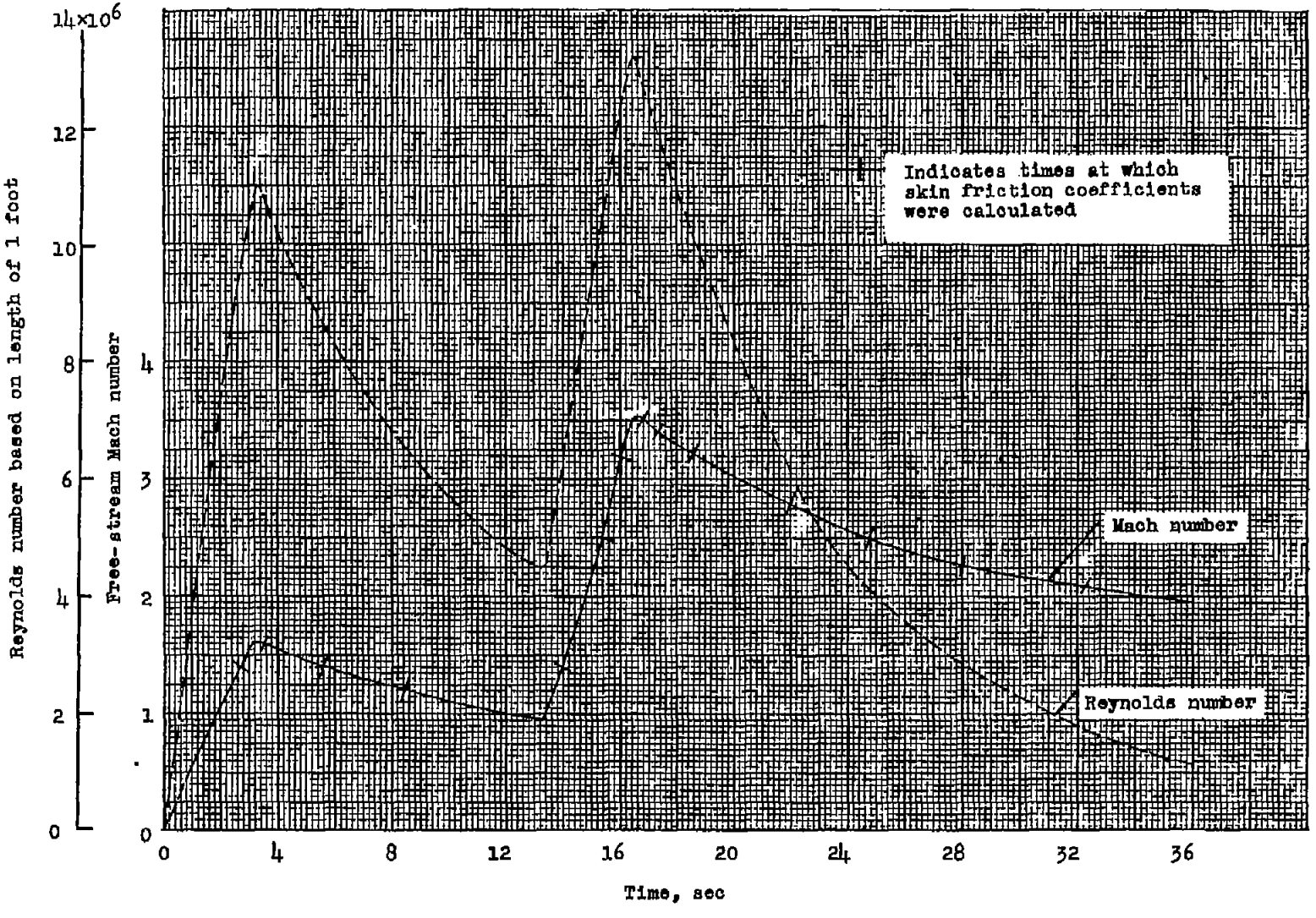

Figure 8.- Time histories of free-stream Mach number and Reynolds number based on length of 1 foot.

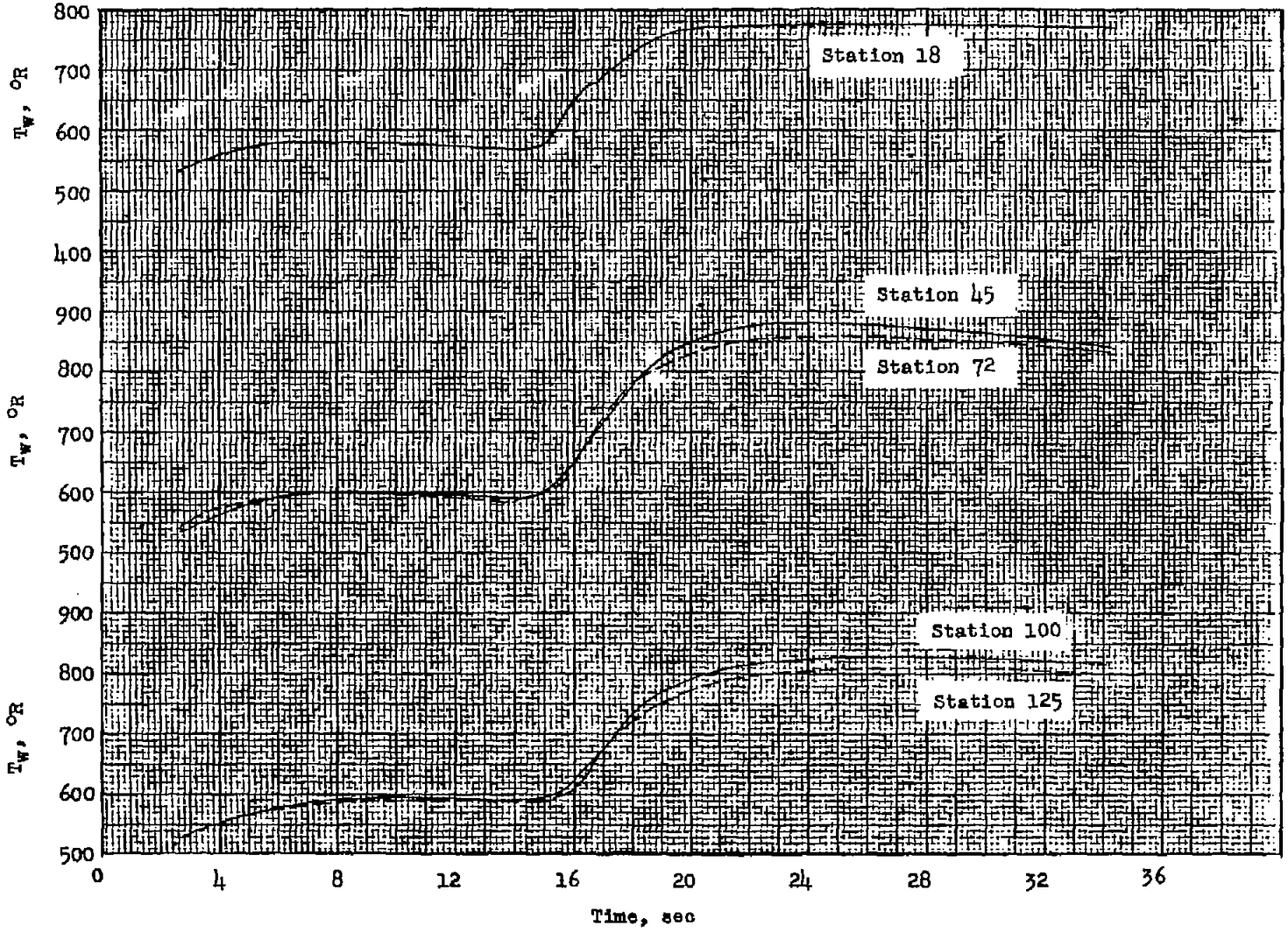

Figure 9.- Time histories of skin temperature.

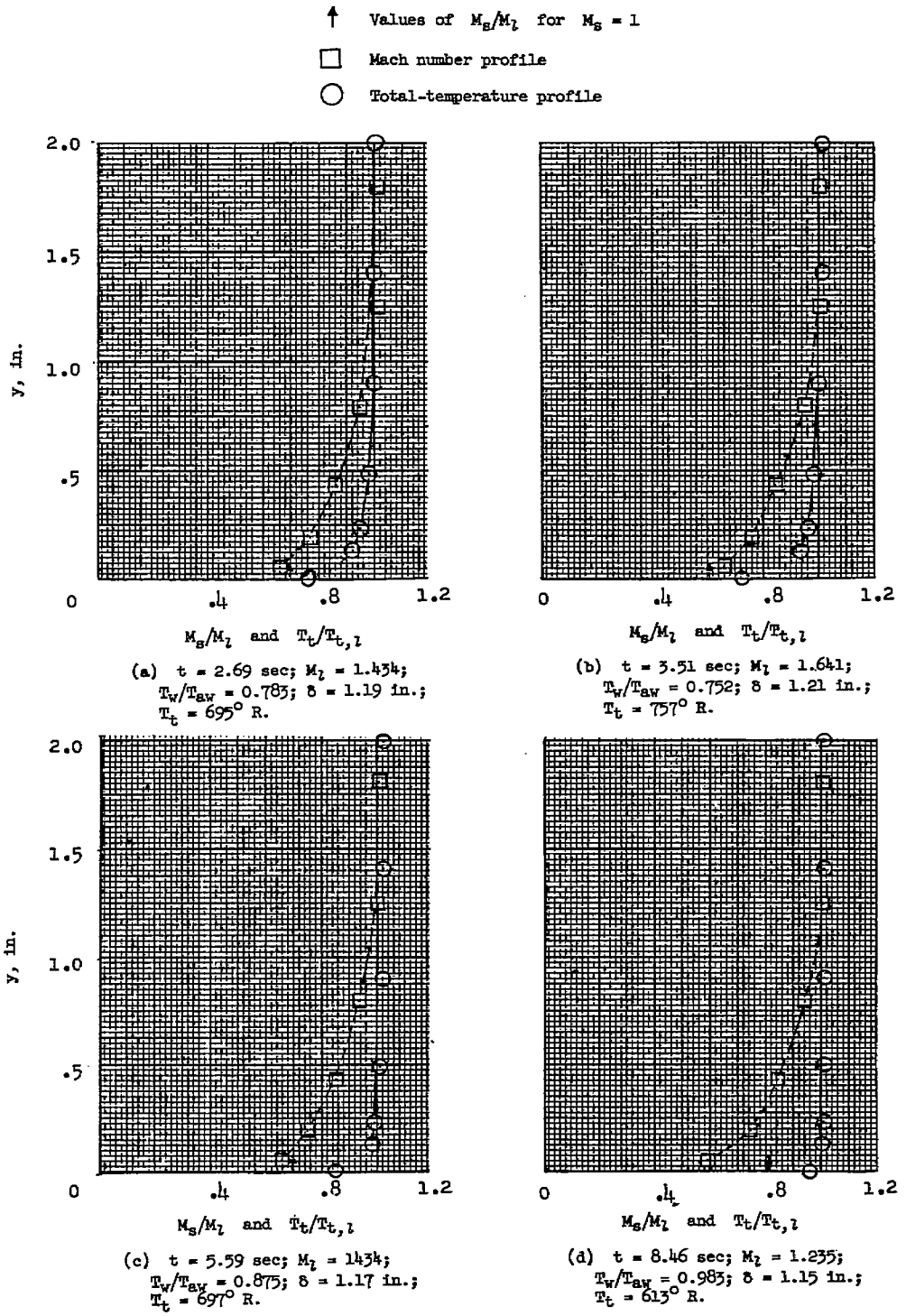

Figure 10.- Mach number and total-temperature profiles.

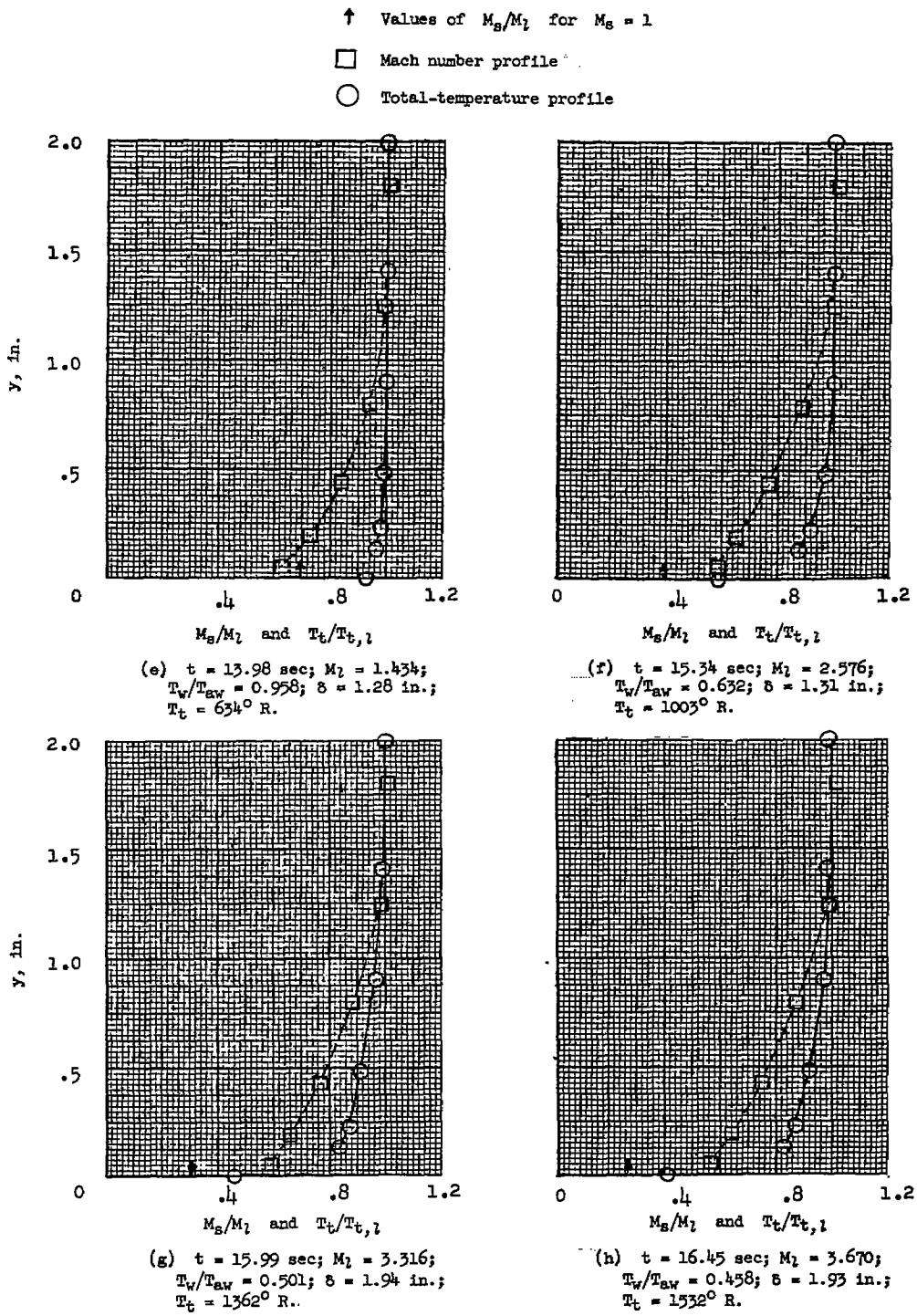

(e) $t = 13.98$ sec; $M_l = 1.434$; $T_w/T_{aw} = 0.958$; $\delta = 1.28$ in.; $T_t = 634^\circ$ R.

(f) $t = 15.34$ sec; $M_l = 2.576$; $T_w/T_{aw} = 0.632$; $\delta = 1.31$ in.; $T_t = 1003^\circ$ R.

(g) $t = 15.99$ sec; $M_l = 3.316$; $T_w/T_{aw} = 0.501$; $\delta = 1.94$ in.; $T_t = 1362^\circ$ R.

(h) $t = 16.45$ sec; $M_l = 3.670$; $T_w/T_{aw} = 0.458$; $\delta = 1.93$ in.; $T_t = 1532^\circ$ R.

Figure 10.- Continued.

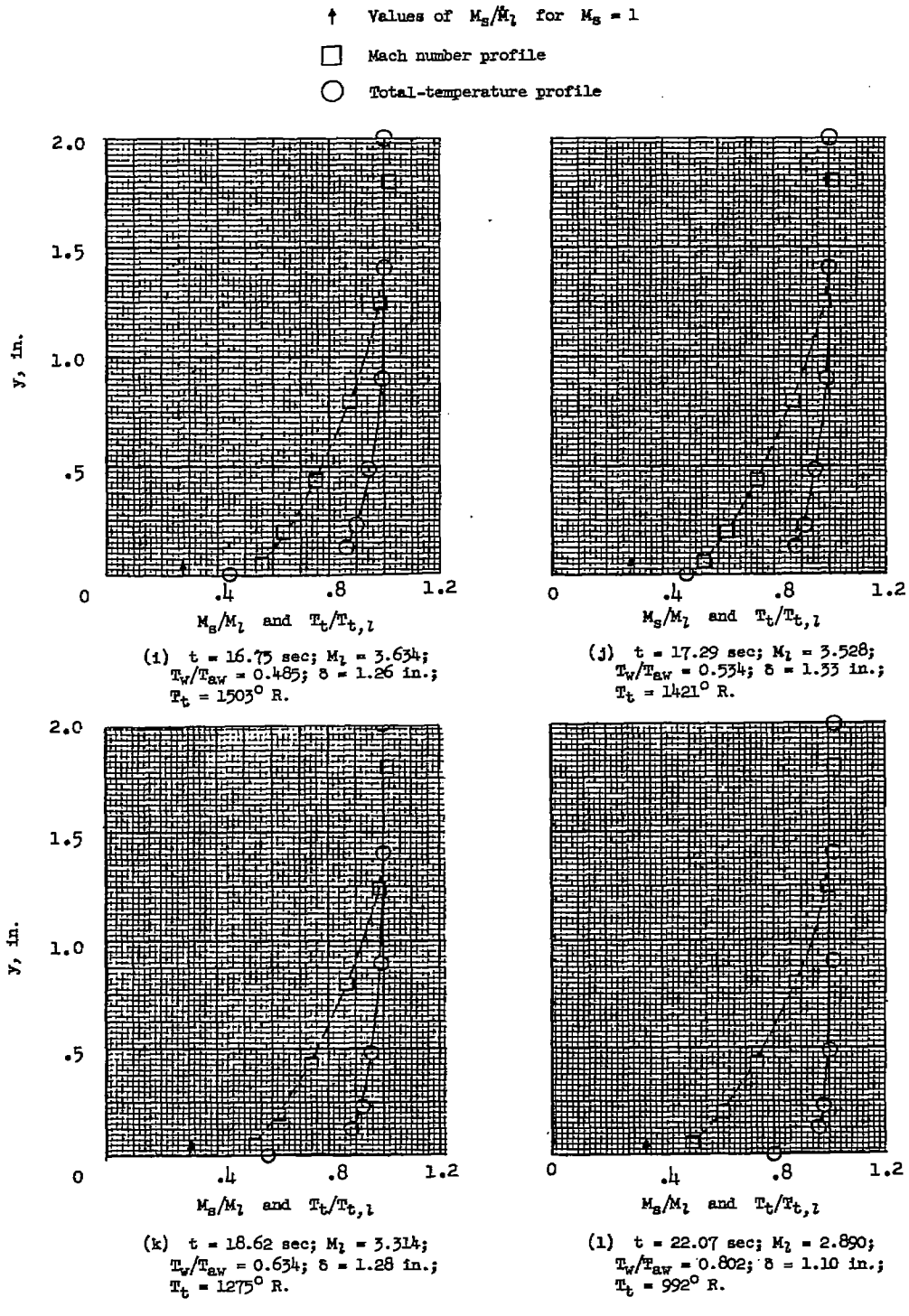

(i) $t = 16.75$ sec; $M_l = 3.634$; $T_w/T_{aw} = 0.485$; $\delta = 1.26$ in.; $T_t = 1503^\circ$ R.

(j) $t = 17.29$ sec; $M_l = 3.528$; $T_w/T_{aw} = 0.534$; $\delta = 1.33$ in.; $T_t = 1421^\circ$ R.

(k) $t = 18.62$ sec; $M_l = 3.314$; $T_w/T_{aw} = 0.634$; $\delta = 1.28$ in.; $T_t = 1275^\circ$ R.

(l) $t = 22.07$ sec; $M_l = 2.890$; $T_w/T_{aw} = 0.802$; $\delta = 1.10$ in.; $T_t = 992^\circ$ R.

Figure 10.- Continued.

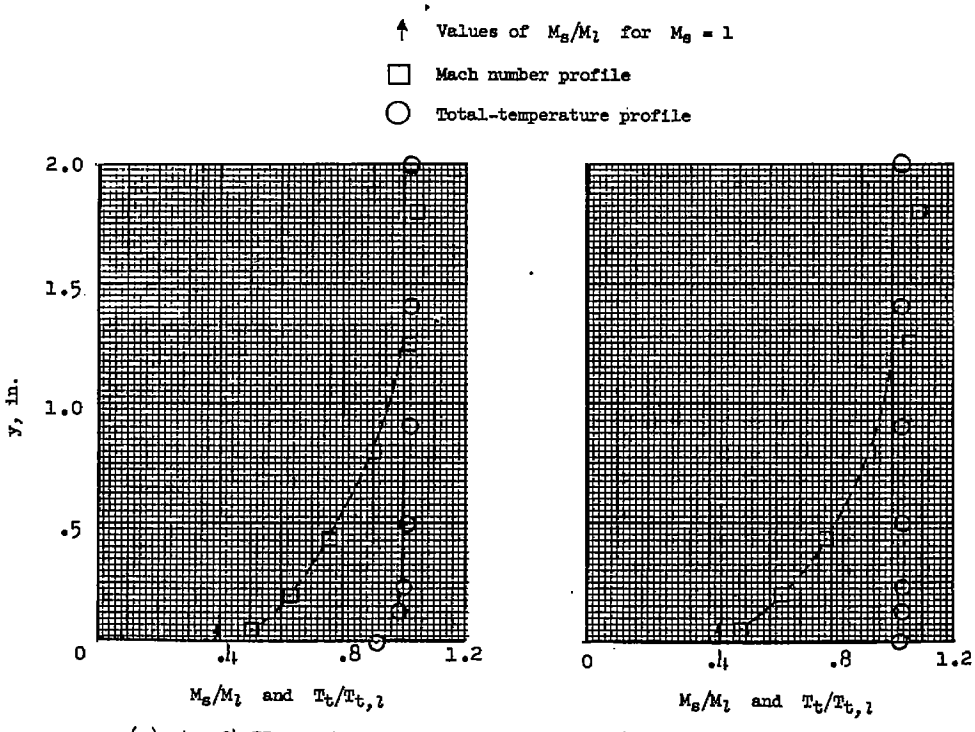

(m) t = 24.75 sec; M_l = 2.573; T_w/T_{aw} = 0.978; δ = 1.07 in.; T_t = 886° R.

(n) t = 28.00 sec; M_l = 2.285; T_w/T_{aw} = 1.093; δ = 0.93 in.; T_t = 790° R.

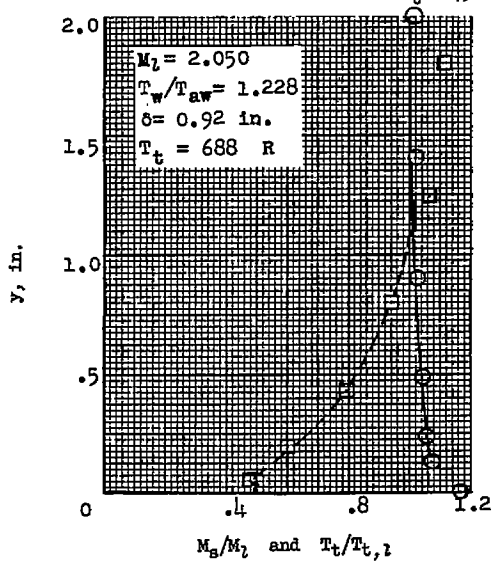

(o) t = 34.17 sec; M_l = 2.050; T_w/T_{aw} = 1.228; δ = 0.92 in.; T_t = 688° R.

Figure 10.- Concluded.

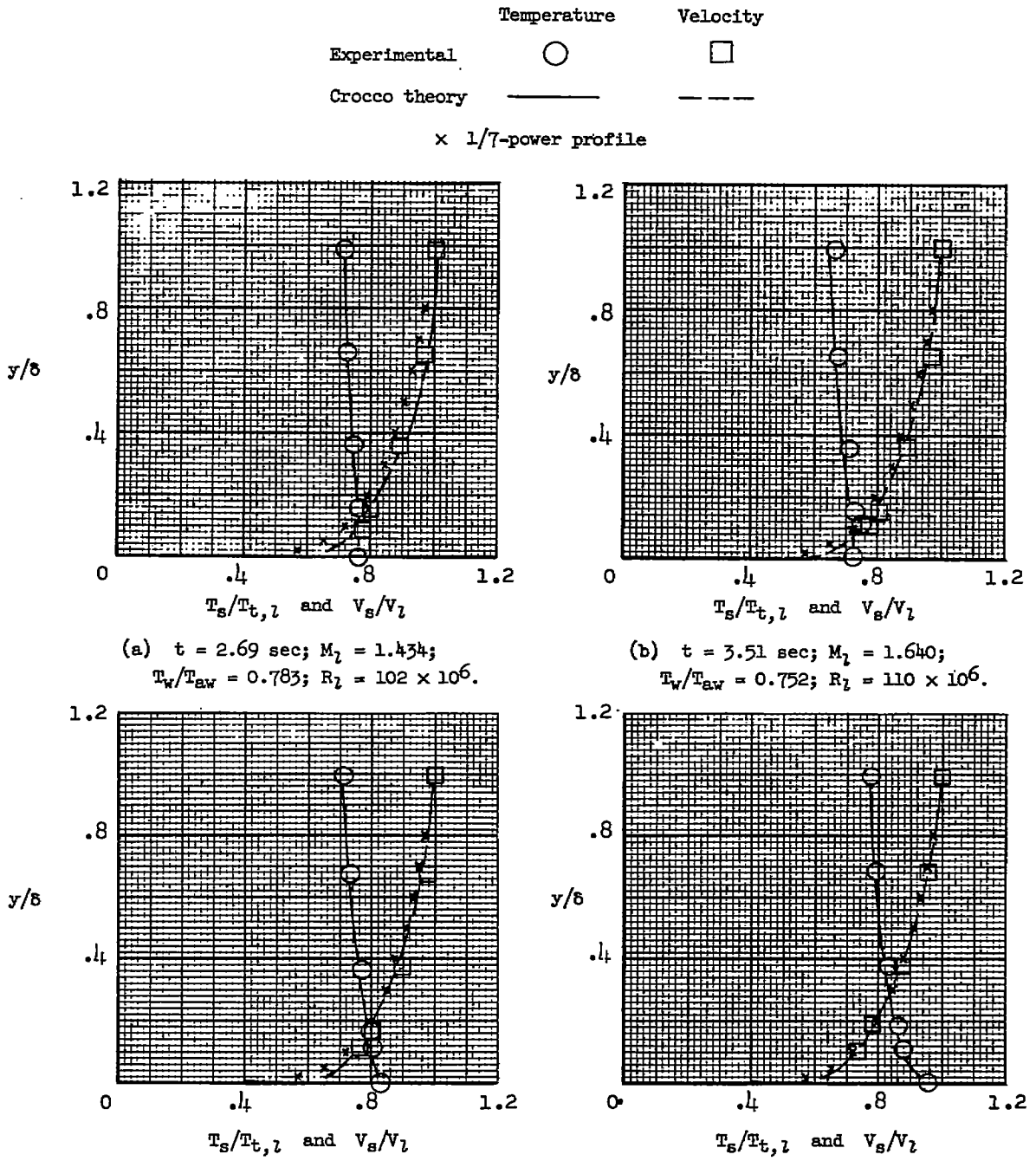

(a) $t = 2.69$ sec; $M_l = 1.434$; $T_w/T_{aw} = 0.783$; $R_l = 102 \times 10^6$.

(b) $t = 3.51$ sec; $M_l = 1.640$; $T_w/T_{aw} = 0.752$; $R_l = 110 \times 10^6$.

(c) $t = 5.59$ sec; $M_l = 1.434$; $T_w/T_{aw} = 0.875$; $R_l = 90 \times 10^6$.

(d) $t = 8.46$ sec; $M_l = 1.235$; $T_w/T_{aw} = 0.983$; $R_l = 68 \times 10^6$.

Figure 11.- Velocity and static-temperature profiles.

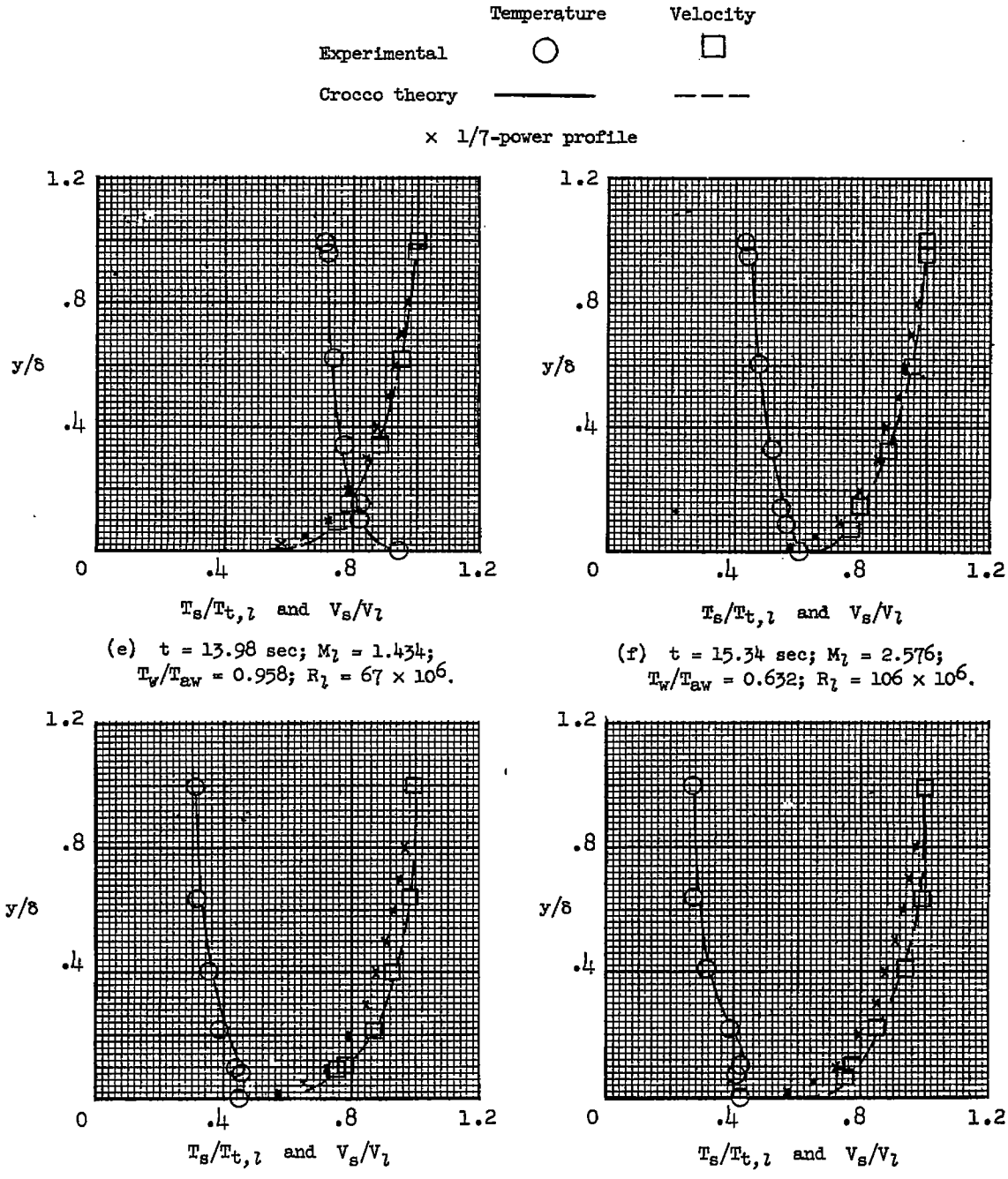

(e) $t = 13.98$ sec; $M_l = 1.434$; $T_w/T_{aw} = 0.958$; $R_l = 67 \times 10^6$.

(f) $t = 15.34$ sec; $M_l = 2.576$; $T_w/T_{aw} = 0.632$; $R_l = 106 \times 10^6$.

(g) $t = 15.99$ sec; $M_l = 3.316$; $T_w/T_{aw} = 0.501$; $R_l = 123 \times 10^6$.

(h) $t = 16.45$ sec; $M_l = 3.670$; $T_w/T_{aw} = 0.458$; $R_l = 124 \times 10^6$.

Figure 11.- Continued.

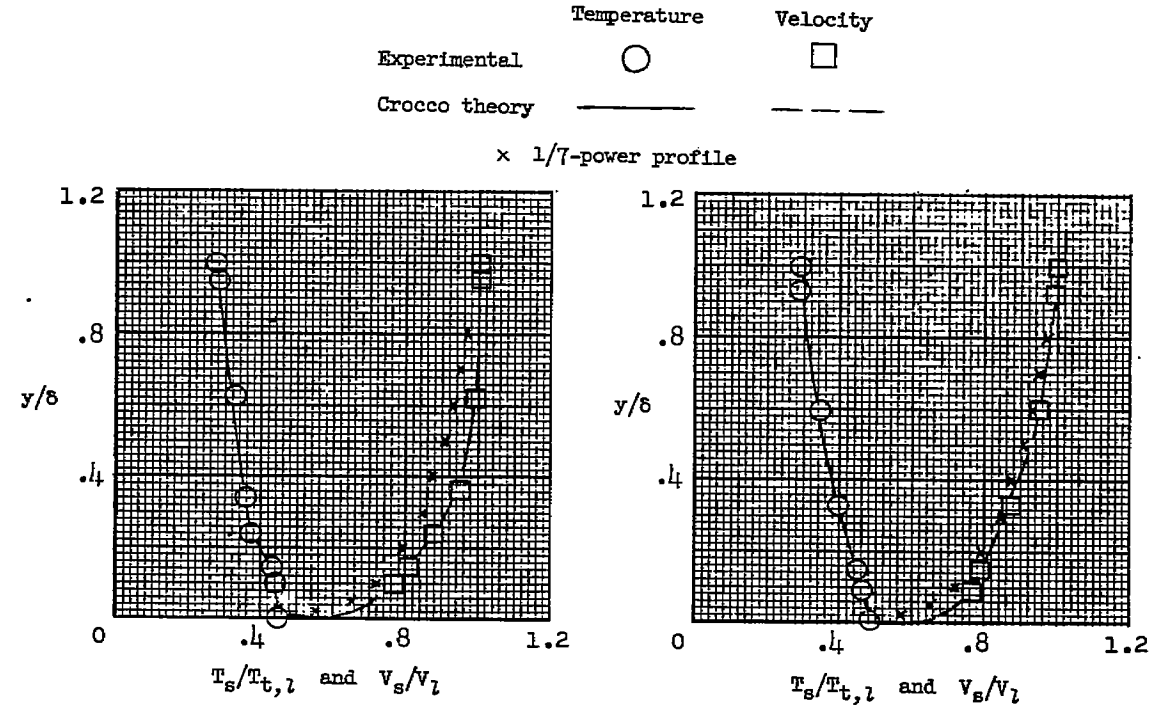

(i) $t = 16.75$ sec; $M_l = 3.634$; $T_w/T_{aw} = 0.485$; $R_l = 123 \times 10^6$.

(j) $t = 17.29$ sec; $M_l = 3.528$; $w/T_{aw} = 0.534$; $R_l = 115 \times 10^6$.

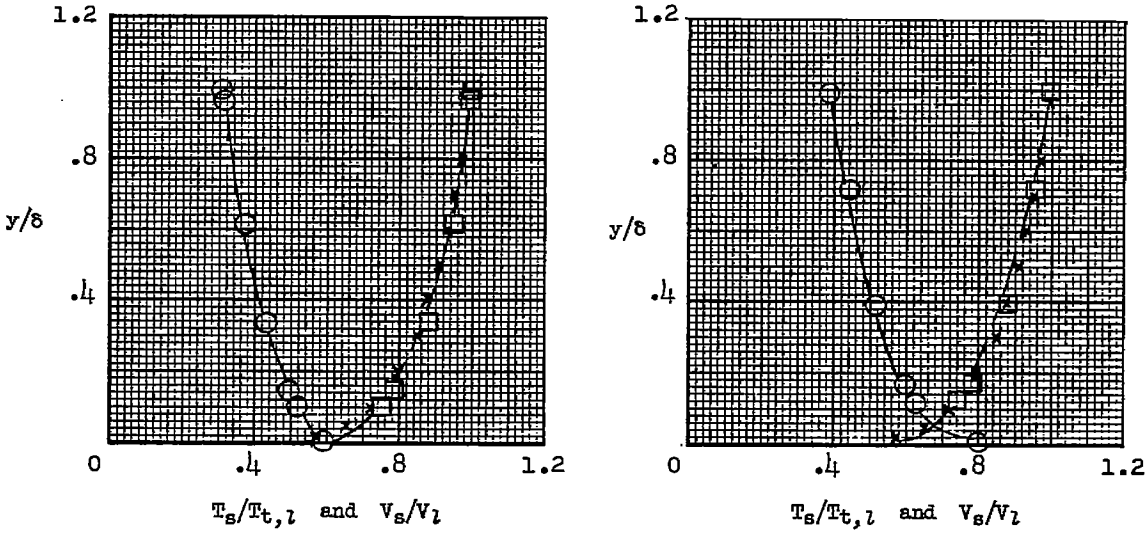

(k) $t = 18.62$ sec; $M_l = 3.314$; $T_w/T_{aw} = 0.634$; $R_l = 94 \times 10^6$.

(l) $t = 22.07$ sec; $M_l = 2.890$; $T_w/T_{aw} = 0.802$; $R_l = 62 \times 10^6$.

Figure 11.- Continued.

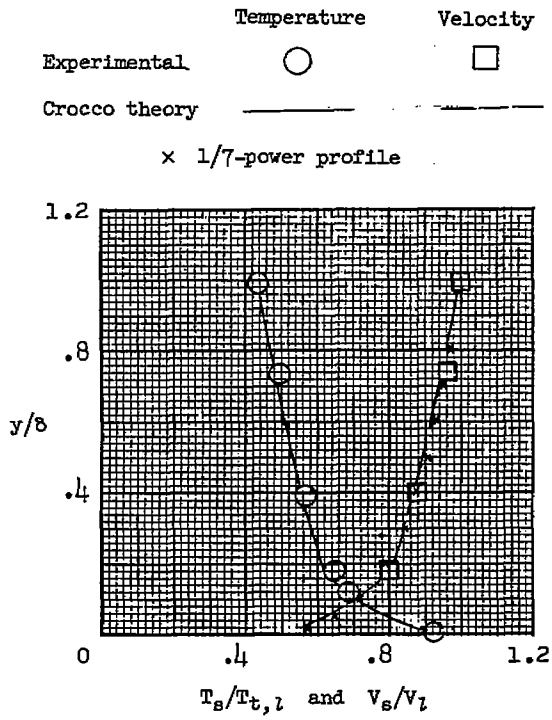

(m) $t = 24.75$ sec; $M_l = 2.573$; $T_w/T_{aw} = 0.978$; $R_l = 42 \times 10^6$.

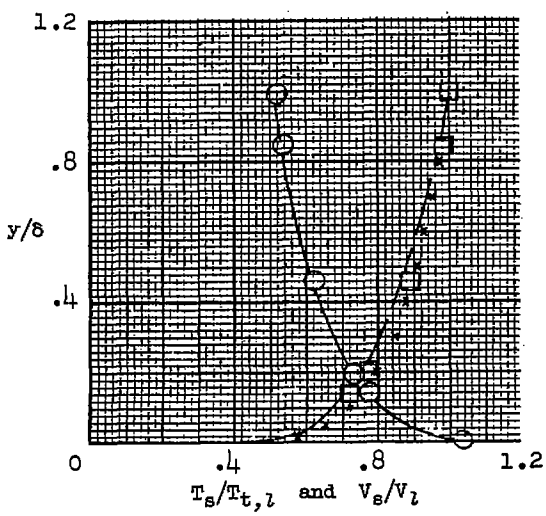

(n) $t = 28.00$ sec; $M_l = 2.285$; $T_w/T_{aw} = 1.093$; $R_l = 26 \times 10^6$.

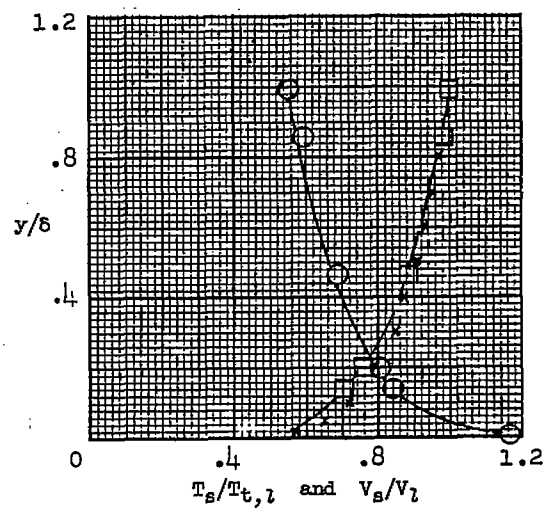

(o) $t = 34.17$ sec; $M_l = 2.050$; $T_w/T_{aw} = 1.228$; $R_l = 15 \times 10^6$.

Figure 11.- Concluded.

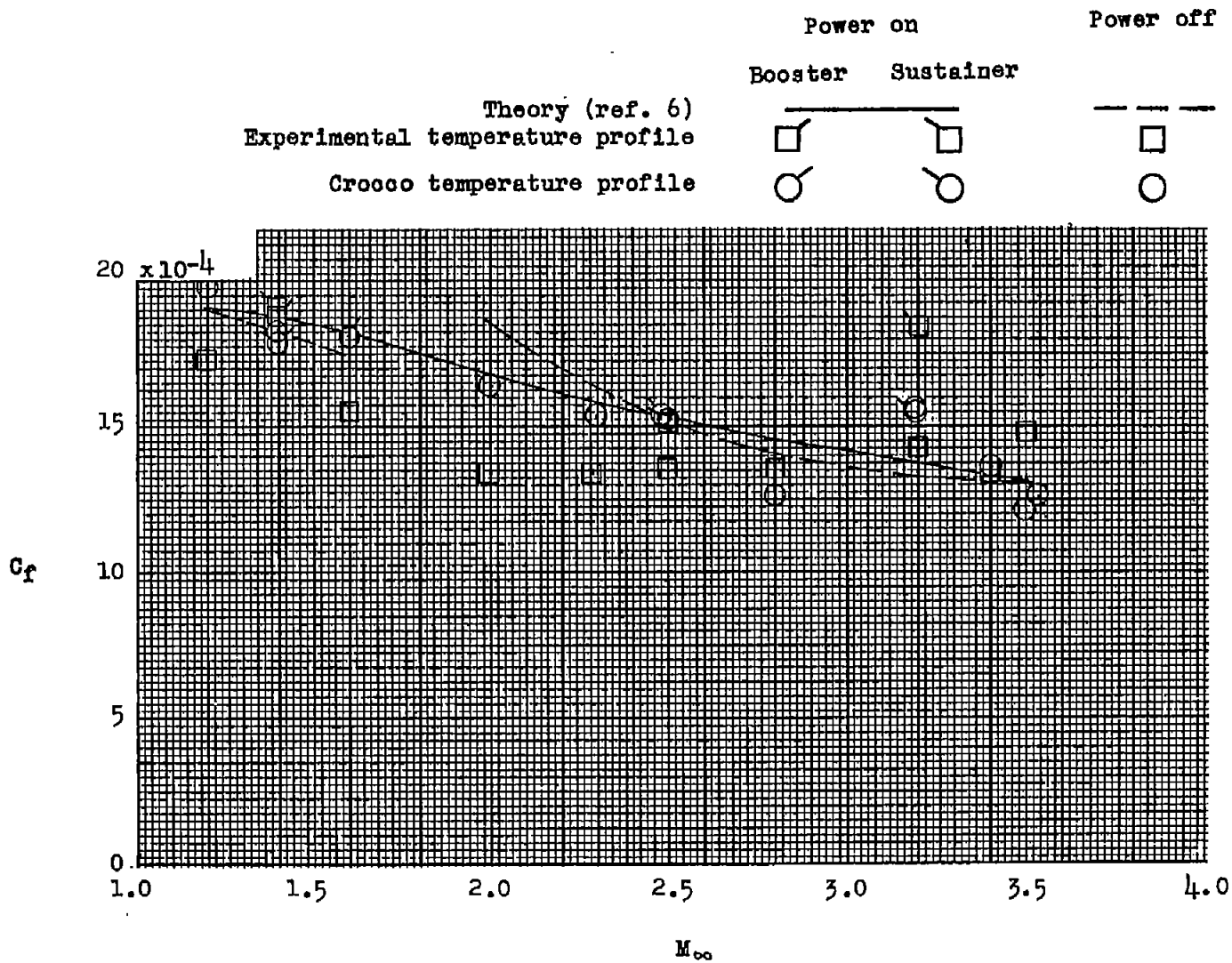

Figure 12.- Variation of skin-friction coefficient with Mach number.

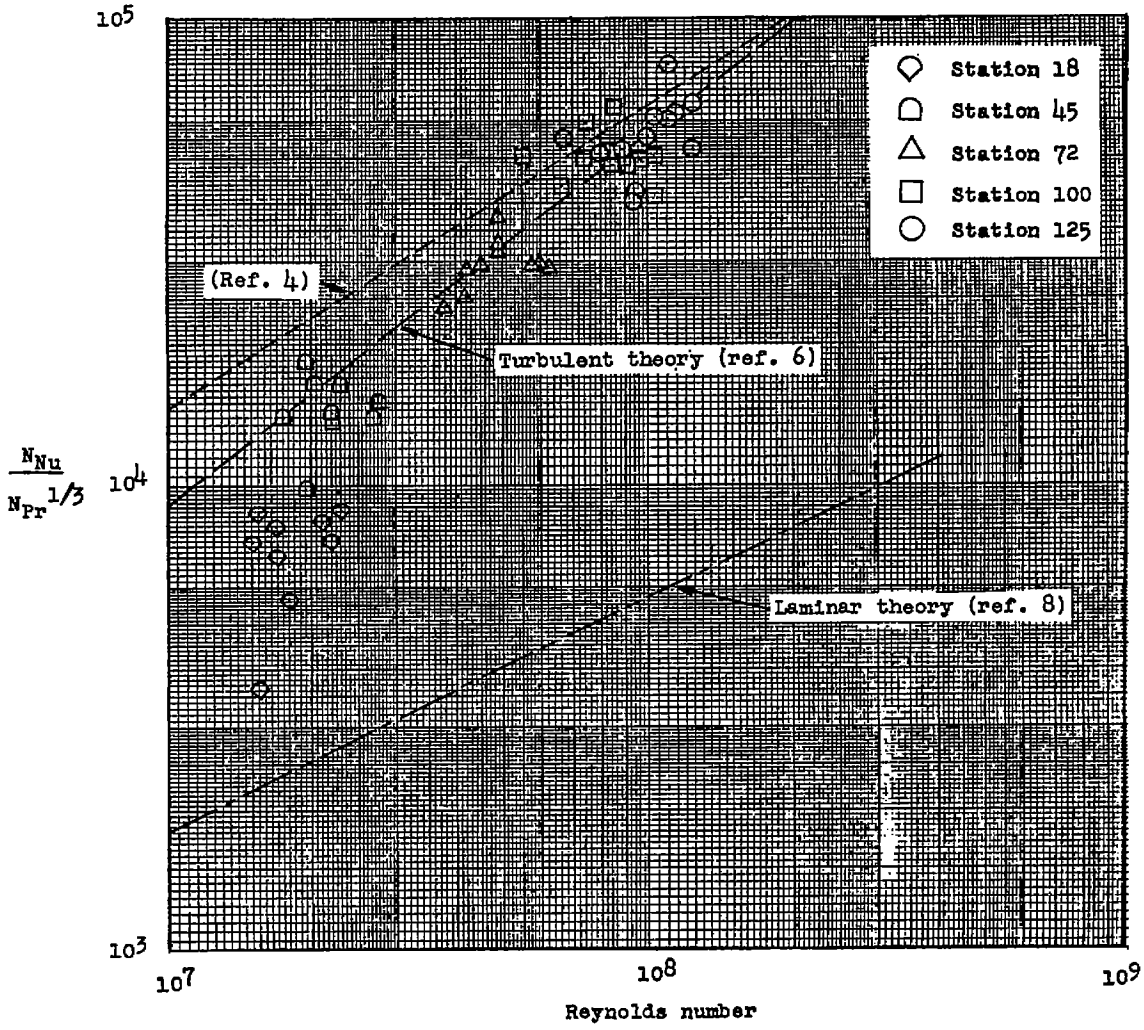

Figure 13.- Heat-transfer measurements.